TRAVELING-WAVE SOLUTIONS AND CHAOTIC DYNAMICS OF THE CONFORMABLE FRACTIONAL SCHRÖDINGER–HIROTA EQUATION

Fengling Ding

Department of Mathematics, Northeast Petroleum University
Daqing, Heilongjiang, 163318, China
sylvia_ding2025@163.com

Received 25 July 2026, accepted 9 October 2026, published online 16 November 2026

This paper examines the dynamical characteristics, chaotic behavior, and traveling-wave solutions of the fourth-order generalized nonlinear fractional Schrödinger–Hirota equation with a conformable fractional derivative. We begin by applying a traveling-wave transformation together with the trial equation method. This reduces the original equation to an ordinary differential equation, which is then framed as a planar Hamiltonian system. The bifurcation analysis of the dynamical system allows us to classify the possible solution types. Corresponding phase portraits visually illustrate these different solution structures. To explore chaotic behavior, we introduce perturbations into the system. The emergence of chaos is confirmed using several indicators: three-dimensional phase plots, time series, and the calculation of positive largest Lyapunov exponents. By combining Liu's trial equation method with the complete discriminant system, we derive ten distinct families of traveling-wave solutions. Three-dimensional graphs clearly illustrate how different fractional-order parameters affect the solution. This work integrates soliton construction with dynamical systems analysis, creating a coherent framework for understanding fractional soliton behavior.

DOI:10.5506/APhysPolB.57.12-A6

1. Introduction

Nonlinear partial differential equations (NPDEs) constitute a key element of modern mathematical physics [1–4] and describe various phenomena across multiple disciplines, including fluid dynamics [5], nonlinear optics, liquid crystals [6], and particle physics [7]. Thus NPDEs are powerful tools for understanding evolution equations and the concept of soliton. NPDEs exhibit more complicated properties and behaviors than linear partial differential equations, which are mainly reflected in chaotic behaviors and bifurcations [8, 9]. The classical nonlinear Schrödinger–Hirota equation (SHE)

forms the theoretical foundation for soliton propagation in optical media. Higher-order dispersion effects require more complex models. The SHE has particular significance in nonlinear optics as it extends the standard framework by combining fourth-order dispersion and nonlinear dispersion terms [10]. Therefore, in this work, we adopt the fourth-order SHE.

Researchers have developed numerous analytical methods for solving nonlinear evolution equations. The tanh-function method [11, 12] and the exp-function method [13] provide systematic approaches for finding traveling-wave solutions. Then the (G'/G)-expansion method [14] and its extensions [15–18] have also been used for various nonlinear models. The modified Kudryashov method [19] finds solutions for equations with polynomial nonlinearities. The Euler–Lagrange variational method has been applied to the time-fractional equation [20] and space-time fractional equation [21–23]. The extended direct algebraic method [24, 25], the Atangana–Baleanu fractional derivative method [26], and the Sardar-sub equation method [27] have also been applied successfully to complex nonlinear systems.

Studies on the integer-order SHE and related nonlinear models have recently greatly improved our understanding of optical soliton dynamics. For instance, Onder adopted the Lie symmetry method as well as the unified Riccati equation expansion method. With these methods, he obtained optical soliton solutions and other kinds of soliton solutions for the model [28]. Li took a different approach. He applied wave transformation together with the complete discriminant system method [29]. As a result, he not only derived optical soliton solutions but also produced three-dimensional, two-dimensional, and contour maps. Du adopted the auxiliary equation method. His goal was to seek various types of exact solutions [30]. Tang studied the dynamics, chaos, and traveling-wave solutions of the perturbed SHE with cubic–quintic–septic nonlinearity using the qualitative theory [31]. He also investigated the SHE in DWDM networks [32] and the generalized stochastic SHE in magneto-optic waveguides [33].

This paper differs from other integer-order works. We considered a fourth-order generalized conformable fractional SHE, which applies to the Schrödinger equation [34]. The parameter $\alpha \in (0, 1]$ directly controls the amplitude and spatial distribution of the resulting traveling-wave solutions. When $\alpha = 1$, the model can be regarded as classical integer-order model. Although the conformable fractional derivative is regarded as a local derivative, it retains the standard chain and product rules of classical calculus, allowing it to be easily simplified to the planar dynamical system analyzed in Section 3. This transformation makes it feasible to study the dynamical and chaotic behaviors, which reflects the physical essence of dynamical characteristics in this research. This is a new insight that cannot be obtained from the integer-order SHE.

The generalized nonlinear fractional SHE takes the form [35]

$$iD_t^\alpha u + d_2 D_x^{2\alpha} u + id_3 D_x^{3\alpha} u + d_4 D_x^{4\alpha} u + ibD_x^\alpha \left(|u|^2 u\right) \\ +\sigma i|u|^2 D_x^\alpha u + i\lambda D_x^\alpha (|u|^2) u = c_1|u|^2 u + c_2|u|^4 u\,, \tag{1}$$

where $u = u(x,t)$ is the wave envelope, with x and t, respectively, denoting spatial and temporal variables. The parameter $\alpha \in (0,1]$ is the fractional order of the system. d_2, d_3, and d_4 are physical coefficients representing dispersion of different orders. The nonlinear terms governed by b, σ, λ, c_1, and c_2 represent self-steepening effects, self-phase modulation, and various Kerr-type nonlinearities.

In recent years, investigations have combined soliton solution methods with dynamical systems analysis [2, 36]. Bifurcation analysis reveals how solution structure changes as parameters vary and identifies critical transitions between different dynamical regimes [37, 38]. Moreover, recent studies have investigated the Schrödinger–Hirota equation via the Riemann–Hilbert analysis [39], and have analyzed bifurcation, chaotic dynamics, and soliton solutions in coupled Fokas–Lenells, stochastic DWDM, and coupled Kaup–Newell systems [40–42]. Although great progress has been made, the fourth-order conformable fractional SHE remains insufficiently explored. Previous works concerning the Jacobi elliptic function method [35, 43] obtained periodic and solitary wave solutions. However, they did not systematically analyze the dynamical behavior. Thus, the chaotic dynamics induced by both external periodic and stochastic perturbations have not yet been studied for this model.

The trial equation method, proposed by Liu [44–46], provides a systematic framework for classifying exact solutions. This approach combines a traveling-wave transformation with complete discrimination systems for polynomials [47]. Compared with other methods, this approach together with the complete discrimination system offers advantages for obtaining a comprehensive classification of exact solutions by taking an integral instead of assuming the solution in advance. To conduct this study, we adopt the trial equation method to solve the fourth-order fractional SHE, and acquire the complete classification of traveling-wave solutions. Bifurcation theory offers a useful perspective for analyzing the resulting system through dynamical system and chaos. The planar dynamical system reveals equilibrium points and phase portraits for different parameters. When external perturbations are introduced into the governing dynamical system, regular motion can change to chaos. Therefore, we introduce periodic and stochastic perturbations. Then, the sensitivity to initial conditions can be shown through the largest Lyapunov exponent (LLE) [48], which is a quantitative indicator used to identify chaotic dynamics, where a positive value confirms

the exponential divergence of nearby trajectories and the presence of chaos. Time series analysis and phase portraits provide different perspectives on the system's complex dynamics. Finally, we present graphical illustrations of representative solutions for different fractional order α.

The motivation of this paper has two aspects. First, the fourth-order SHE is an important model in optics and the conformable fractional derivative is a tool that has been widely used to describe memory and nonlocal effects. Second, although the integer-order form has been extensively investigated, the dynamical and chaotic properties of its fractional model have not yet been studied. In particular, the influence of the fractional order on soliton behavior has not been systematically examined.

The contributions of this paper are that we derive ten families of traveling-wave solutions and analyze the dynamical system and chaotic behaviors. This paper also has several contributions. We extend the SHE to the conformable fractional SHE. We analyze the system as a planar Hamiltonian dynamical system and study its equilibrium types and phase portraits. Then, we add three perturbations and show chaotic behaviors via phase portraits, time series, and positive LLE. We obtain traveling-wave solutions and show representative solutions for different fractional orders. The main novelty is that we combine the conformable fractional SHE with traveling-wave solutions, dynamical analysis, and chaotic behaviors. These results provide a coherent framework that can help us to understand fractional soliton behavior.

The paper is organized as follows. Section 2 is the mathematical analysis, transforming Eq. (1) into an ordinary differential system and deriving key relations. Section 3 presents the bifurcation analysis, which include dynamical characteristics and chaotic behavior. Section 4 provides the quantitative analysis with explicit exact solutions and graphical representations. Section 5 concludes with a overview of findings.

2. Mathematical analysis

In order to convert the time fractional partial differential equation into an ordinary differential equation, we use the following transformation for Eq. (1) [35]:

$$u(x,t)=\eta(\xi)\,\mathrm{e}^{i\left(\kappa\frac{x^{\alpha}}{\alpha}-\tau\frac{t^{\alpha}}{\alpha}-\theta_0\right)},\qquad \xi=\frac{x^{\alpha}}{\alpha}-v\frac{t^{\alpha}}{\alpha}. \tag{2}$$

where $\eta(\xi)$ represents the amplitude component, κ is the carrier wave number, τ is the temporal frequency shift, θ_0 is the initial phase, and v is the wave envelope propagation velocity.

Now, we substitute above equation into Eq. (1) and decompose it into the real and imaginary parts. The real component yields

$$d_4\eta_\xi^{(4)} + \left(d_2 - 3d_3\kappa - 6d_4\kappa^2\right)\eta_\xi'' + \left(d_4\kappa^4 + d_3\kappa^3 - d_2\kappa^2 - \tau\right)\eta - \left(c_1 + \kappa\lambda + b\kappa\right)\eta^3 - c_2\eta^5 = 0\,, \tag{3}$$

while the imaginary component gives

$$\left(d_3 + 4d_4\kappa\right)\eta_\xi''' + \left(\lambda + 2\sigma + 3b\right)\eta^2\eta_\xi - \left(v - 2d_2\kappa + 3d_3\kappa^2 + 4d_4\kappa^3\right)\eta_\xi = 0\,. \tag{4}$$

By examining the imaginary component, we obtain the soliton speed

$$v = 2d_2\kappa - 3d_3\kappa^2 - 4d_4\kappa^3\,, \tag{5}$$

and the frequency

$$\kappa = -\frac{d_3}{4d_4}\,. \tag{6}$$

We simplify Eq. (3)

$$\eta^{(4)} + A_1\eta'' + A_2\eta - A_3\eta^3 - A_4\eta^5 = 0\,, \tag{7}$$

with

$$\begin{aligned} A_1 &= \frac{d_2 - 3d_3\kappa - 6d_4\kappa^2}{d_4}\,, \\ A_2 &= \frac{d_4\kappa^4 + d_3\kappa^3 - d_2\kappa^2 - \tau}{d_4}\,, \\ A_3 &= \frac{c_1 + \kappa\lambda + b\kappa}{d_4}\,, \\ A_4 &= \frac{c_2}{d_4}\,. \end{aligned}$$

To construct exact traveling-wave solutions, we employ the trial equation method combined with the complete discriminant system for polynomials. According to Liu trial equation [44], substituting $\eta'' = \sum_{i=0}^{n} d_i u^i(\xi)$ into Eq. (7), we obtain

$$\eta'' = a_3\eta^3 + a_2\eta^2 + a_1\eta + c_0\,, \tag{8}$$

and

$$\left(\eta'\right)^2 = \frac{1}{2}a_3\eta^4 + \frac{2}{3}a_2\eta^3 + a_1\eta^2 + 2a_0\eta + 2c_0\,, \tag{9}$$

with

$$
\begin{aligned}
a_3 &= \pm\sqrt{\frac{A_4}{6}}\,,\\
a_2 &= 0\,,\\
a_1 &= \pm\frac{A_3\sqrt{6}}{10\sqrt{A_4}} - \frac{A_1}{10}\,,\\
a_0 &= 0\,,\\
c_0 &= \mp\frac{1}{12}\left(\frac{1}{\sqrt{\frac{A_4}{6}}}\right)\left[\left(\pm\frac{A_3\sqrt{6}}{10\sqrt{A_4}} - \frac{A_1}{10}\right)^2 + A_1\left(\pm\frac{A_3\sqrt{6}}{10\sqrt{A_4}} - \frac{A_1}{10}\right) + A_2\right]\,.
\end{aligned}
$$

3. Bifurcation analysis

The focus now shifts to the analysis of Eq. (9) using bifurcation theory. The analysis is divided into two subsections: the dynamical characteristics and the chaotic behavior. All figures are plotted using MATLAB.

3.1. Dynamical characteristics

Equation (9) can be expressed as [49–54]

$$
\begin{cases}
\frac{\mathrm{d}\eta}{\mathrm{d}\xi} &= Z\,,\\
\frac{\mathrm{d}Z}{\mathrm{d}\xi} &= a_3\eta^3 + a_1\eta\,,
\end{cases}
\tag{10}
$$

hence, the Hamiltonian is given by

$$
H(\eta, Z) = \frac{Z^2}{2} - \left(\frac{1}{4}a_3\eta^4 + \frac{1}{2}a_1\eta^2 + \frac{1}{2}c_0\right)\,,
\tag{11}
$$

with $\frac{\partial H}{\partial Z} = \eta'$, $\frac{\partial H}{\partial \eta} = -Z'$. Z represents generalized momentum and η symbolizes generalized coordinate. Then, we have the total derivative in the following form:

$$
\begin{aligned}
\frac{\mathrm{d}H}{\mathrm{d}\xi} &= \frac{\partial H}{\partial \eta}\frac{\mathrm{d}\eta}{\mathrm{d}\xi} + \frac{\partial H}{\partial Z}\frac{\mathrm{d}Z}{\mathrm{d}\xi}\\
&= -Z'Z + \eta'\left(a_3\eta^3 + a_1\eta\right) = 0\,,
\end{aligned}
\tag{12}
$$

thus, $H(\eta, Z) = C$, where C is a constant.

Therefore, from the Hamiltonian Eq. (11), we identify the potential energy function as the part depending solely on η. We obtain the potential energy as follows:

$$F(\eta) = -\left(\frac{1}{4}a_3\eta^4 + \frac{1}{2}a_1\eta^2 + \frac{1}{2}c_0\right) . \tag{13}$$

Then, we need to study the dynamics of Eq. (13), for which we should analyze the roots of $F'(\eta)$

$$\begin{aligned} F'(\eta) &= -\left(a_3\eta^3 + a_1\eta\right) \\ &= -a_3\eta\left(\eta^2 + \frac{a_1}{a_3}\right) , \end{aligned} \tag{14}$$

where, obviously, $a_3 \neq 0$. Now we can use the discrimination of the second-order degree polynomial.

Case 1

When $a_1 = 0$, we have

$$F'(\eta) = -a_3\eta^3 . \tag{15}$$

The system has a unique equilibrium point at the origin. When $a_3 < 0$, we take $a_3 = -1$, $a_1 = 0$. Figure 1 (a) shows that the global phase portrait exhibits a family of nested closed orbits encircling the center point, which indicates that the equation has periodic solutions. When $a_3 > 0$, we take $a_3 = 1$, $a_1 = 0$. Figure 1 (b) shows that the equation has torsional wave solutions.

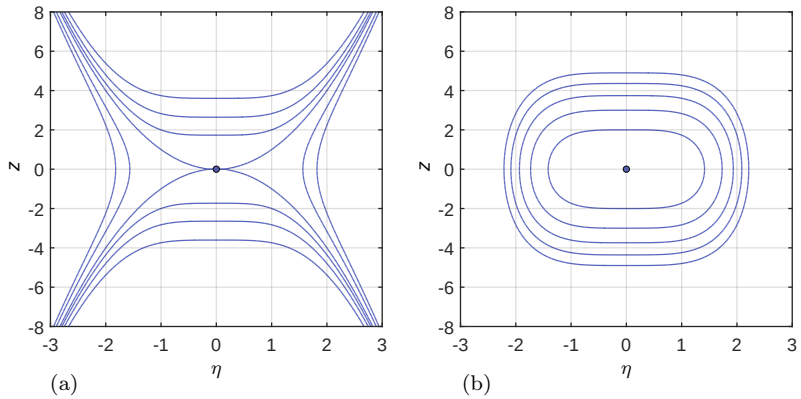


Fig. 1. Phase portrait of the system: (a) $a_3 = -1$, $a_1 = 0$, (b) $a_3 = 1$, $a_1 = 0$.

Case 2

When $\frac{a_1}{a_3} < 0$, we get

$$F'(\eta) = -a_3\eta\,(\eta - \beta_1)\,(\eta - \beta_2)\ , \tag{16}$$

with $\beta_1 < \beta_2$ satisfying $\beta_1 + \beta_2 = 0$. The stability properties of these points depend on the sign of a_3. In Fig. 2 (a), we take $a_3 = 1$, $a_1 = -4$. The origin serves as a center surrounded by periodic orbits, while the points $(\pm 2, 0)$ are saddle points. This shows the existence of kink and anti-kink solitary solutions. In contrst, Fig. 2 (b) presents $a_3 = -1$, $a_1 = 4$. The origin becomes a saddle point, and the two symmetric equilibria $(\pm 2, 0)$ are centers, which shows that the equation has bell-shaped and anti-bell soliton solutions.

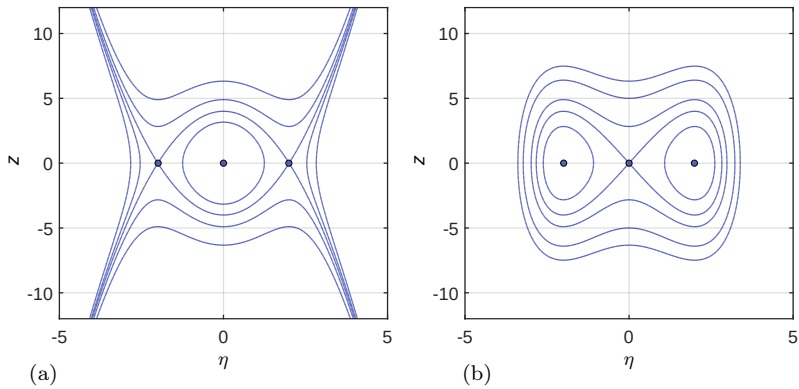


Fig. 2. Phase portrait of the system: (a) $a_3 = 1$, $a_1 = -4$, (b) $a_3 = -1$, $a_1 = 4$.

Case 3

When $\frac{a_1}{a_3} > 0$, we have

$$F'(\eta) = -a_3\eta\left(\eta^2 + \frac{a_1}{a_3}\right)\ . \tag{17}$$

In this case, no additional real roots exist beyond $\eta = 0$. Thus, the dynamical behavior reduces to Case 1, with only one equilibrium point at the origin.

In addition, these specific parameter values are chosen to represent the qualitatively distinct dynamical regimes identified in Cases 1–2: $a_3 < 0$ produces center-type equilibria with periodic orbits, while $a_3 > 0$ yields saddle-center configurations. In summary, under the condition that the solution exists, by exploiting the dynamical characteristics of the equation, we can determine what kind of solution it possesses.

3.2. Chaotic behavior

Chaotic behavior cannot arise from the preceding analysis of the dynamical system [55, 56]. Therefore, we can analyze the chaotic behavior of Eq. (9) by adding the disturbance term $M(\xi)$

$$\begin{cases} \frac{\mathrm{d}\eta}{\mathrm{d}\xi} & = Z\,, \\ \frac{\mathrm{d}Z}{\mathrm{d}\xi} & = a_3\eta^3 + a_1\eta + M(\xi)\,. \end{cases} \tag{18}$$

We now study three types of external perturbations: a sinusoidal function, a cosinusoidal function, and Gaussian noise.

Example 1: sinusoidal perturbation

When $M(\xi) = -0.2\sin(0.3\xi)$, the parameters are set to $a_3 = -1.2$ and $a_1 = -0.5$. The phase portraits in Fig. 3 (a) indicate that the regular track structure has been completely disrupted. The periodic external force input causes the system's response to become unstable and tangled, which confirms that sinusoidal excitation can effectively push the system into non-periodic motion. From Fig. 3 (b), the variation of η over time shows irregular

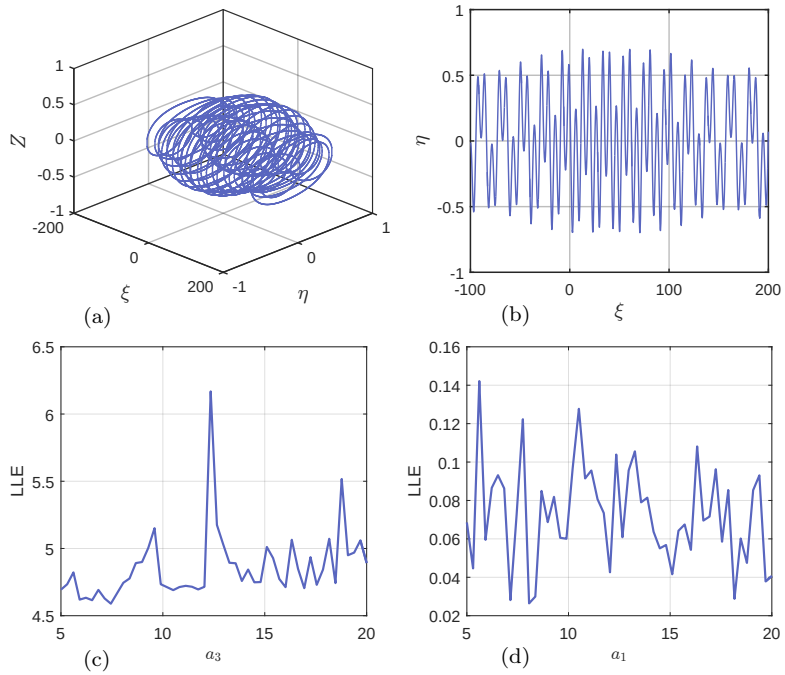


Fig. 3. (a) Phase portrait, (b) time series, and (c) and (d) largest Lyapunov exponents (LLEs) for $a_3 = -1.2$ and $a_1 = -0.5$.

oscillations, with both amplitude and frequency being unstable. Figures 3 (c) and 3 (d) show the LLE for a_3 and a_1, respectively. They are positive, which is the typical characteristics of chaotic motion. The positive exponent indicates that the adjacent trajectories diverge exponentially and the system is chaotic.

Example 2: cosinusoidal perturbation

When $M(\xi) = -0.6\cos(0.5\xi)$, the system parameters are also $a_3 = -1.2$ and $a_1 = -0.5$. Figure 4 (a) shows that the phase trajectories form a complex network structure, causing the system to generate stable nonperiodic oscillations. From Fig. 4 (b), the time series signal shows nonstationary characteristics, with irregular fluctuations occurring. This further confirms the nonperiodicity of the system's motion. From Figs. 4 (c) and 4 (d), the calculated results of LLEs also show positive values. This confirms that cosinusoidal perturbation can also induce chaos. The characteristics are similar to those of sinusoidal perturbation, but the values of the positive exponents and phase portraits are slightly different, reflecting the subtle influence of the different perturbations.

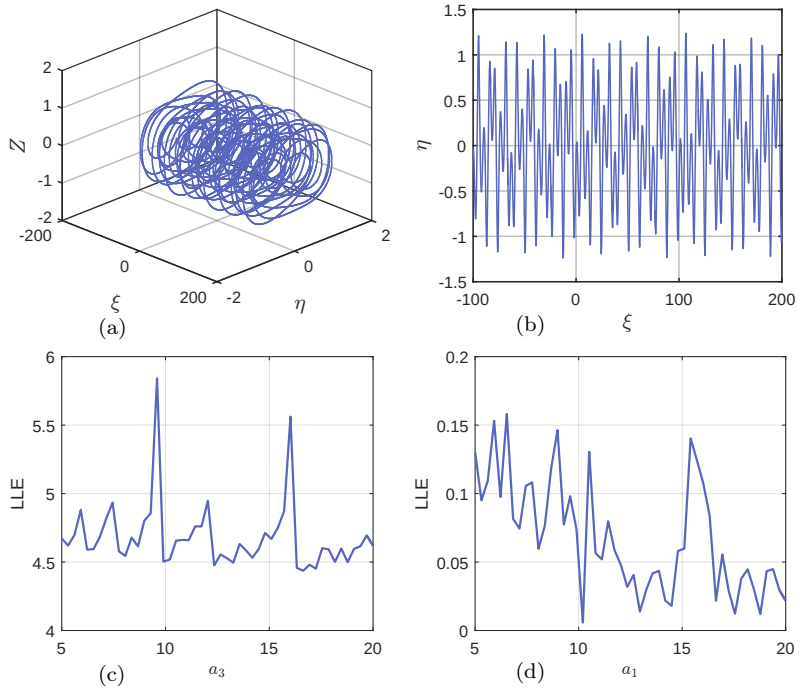


Fig. 4. (a) Phase portrait, (b) time series, and (c) and (d) largest Lyapunov exponents (LLEs) for $a_3 = -1.2$ and $a_1 = -0.5$.

Example 3: Gaussian noise perturbation

When $M(\xi) = 0.4\,\mathrm{e}^{-\xi^2}$, the system parameters are set to $a_3 = -1.2$ and $a_1 = -0.5$. Unlike the deterministic periodic perturbations considered in Examples 1 and 2, this stochastic perturbation introduces random forcing into the dynamical system. The phase portrait in Fig. 5 (a) exhibits a diffuse and disordered trajectory structure, indicating that the system has been driven into a strongly non-periodic state. The random external input causes the system's response to become completely irregular, which confirms that Gaussian excitation can also effectively push the system into chaotic motion. From Fig. 5 (b), the variation of η over time shows highly irregular fluctuations with both amplitude and frequency remaining unpredictable. From Figs. 5 (c) and 5 (d), the LLE values with respect to a_3 and a_1 are positive throughout the scanned parameter ranges, which is the typical characteristics of chaotic motion. The positive exponents confirm that adjacent trajectories diverge exponentially even under stochastic forcing, establishing that the system's chaotic behavior is robust and persists under Gaussian noise perturbation.

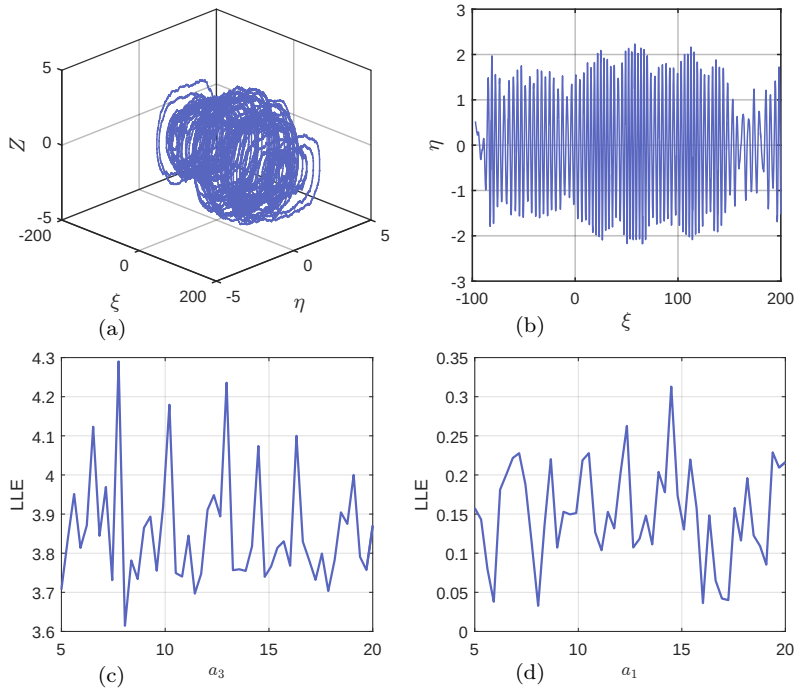


Fig. 5. (a) Phase portrait, (b) time series, and (c) and (d) largest Lyapunov exponents (LLEs) for $a_3 = -1.2$ and $a_1 = -0.5$.

In this section, $a_3 = -1.2$ and $a_1 = -0.5$ were chosen to place the system in a regime where periodic and stochastic perturbations induce chaos, as confirmed by the positive LLE values obtained. In the above three examples, chaotic behavior can be clearly observed from Figs. 3, 4, and 5, and it is also evident that a_3 is obviously greater than a_1, showing that a_3 has a greater impact on the system dynamics. Additionally, we have demonstrated the different effects of different disturbance terms on the dynamical system through phase portraits and LLEs.

4. Quantitative analysis

In this section, in order to transform Eq. (9) to a standard elliptic integral form that conforms to the complete discriminant system and normalize the leading coefficient in the resulting polynomial to unity, we make the following transformation:

$$Q = \eta^2\,, \qquad \omega = \mu\eta^2\,, \qquad \mu = (2a_3)^{\frac{1}{3}}\,. \tag{19}$$

Then Eq. (9) becomes

$$\begin{aligned} \left(Q'\right)^2 &= \omega^3 + m\omega^2 + n\omega \\ &= \omega\left(\omega^2 + m\omega + n\right)\,, \end{aligned} \tag{20}$$

with

$$\begin{aligned} m &= \frac{4a_1}{\mu^2}\,, \\ n &= \frac{6c_0}{\mu}\,. \end{aligned}$$

We simplify Eq. (20) and then integrate it. We obtain

$$\pm(\xi - \xi_0) = \int \frac{\mathrm{d}\omega}{\omega\left(\omega^2 + m\omega + n\right)}\,. \tag{21}$$

We then have the discriminant system for the second-order polynomial

$$\Delta = m^2 - 4n\,. \tag{22}$$

Based on the number of roots of $\omega^2 + m\omega + n$, we can discuss the following several cases. In this section, each solution figure comes with a set of parameter values, which are chosen to satisfy the relevant discriminant conditions (for instance, $\Delta = 0$ and $m < 0$). To show the main characteristics of solutions, we plot only representative solutions from each mathematical form, including hyperbolic, elliptic, and trigonometric.

Case 1

When $\Delta = 0$ and $m < 0$, Eq. (20) is $f(\omega) = \omega(\omega - \gamma)^2$, and the solution of Eq. (1) is

$$u_1 = \left(\pm\sqrt{\frac{2A_4}{3}}\right)^{-\frac{1}{3}} \left[-\frac{m}{2}\tanh^2\left(\frac{1}{2}\sqrt{-\frac{m}{2}}\left(\pm\sqrt{\frac{2A_4}{3}}\right)^{\frac{1}{3}}(\xi-\xi_0)\right)\right]^{\frac{1}{2}} \times \mathrm{e}^{i\left(\kappa\frac{x^\alpha}{\alpha}-\tau\frac{t^\alpha}{\alpha}-\theta_0\right)}, \tag{23}$$

$$u_2 = \left(\pm\sqrt{\frac{2A_4}{3}}\right)^{-\frac{1}{3}} \left[-\frac{m}{2}\coth^2\left(\frac{1}{2}\sqrt{-\frac{m}{2}}\left(\pm\sqrt{\frac{2A_4}{3}}\right)^{\frac{1}{3}}(\xi-\xi_0)\right)\right]^{\frac{1}{2}} \times \mathrm{e}^{i\left(\kappa\frac{x^\alpha}{\alpha}-\tau\frac{t^\alpha}{\alpha}-\theta_0\right)}. \tag{24}$$

Figure 6 illustrates the solution u_1 for different fractional orders $\alpha = 0.3$ and 0.8, with $x = 1$ and $t = 3$.

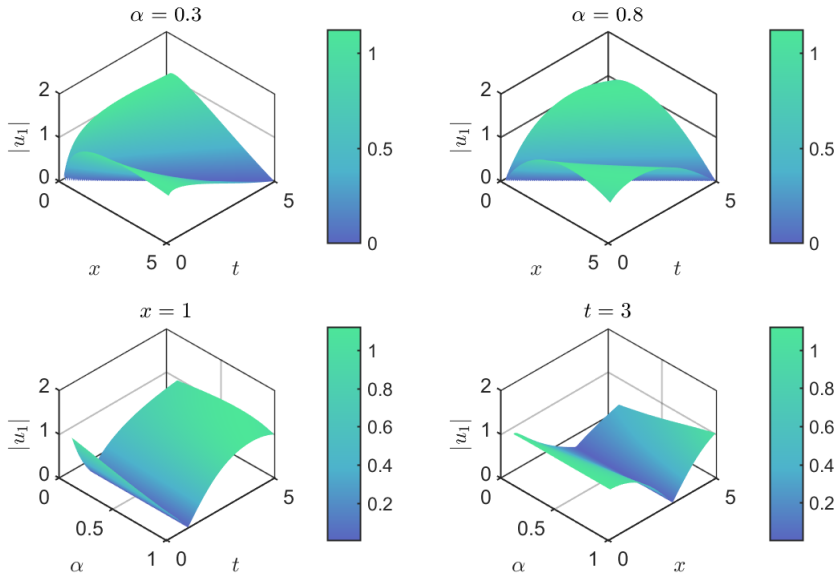


Fig. 6. Surface plots of the modulus $|u_1|$ under fixed parameters $A_4 = 6, m = -1, \xi = 1, \xi_0 = 0, \kappa = 1, \tau = 1, \theta_0 = 0$.

Figure 7 illustrates the solution u_2 for different fractional orders $\alpha = 0.3$ and 0.8.

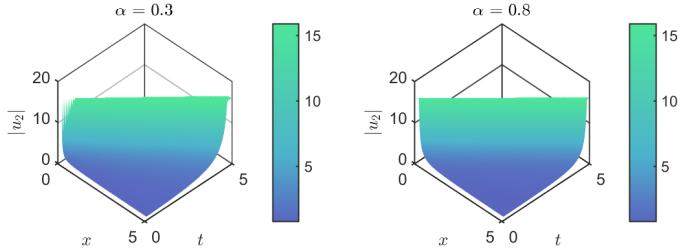


Fig. 7. Surface plots of the modulus $|u_2|$ under fixed parameters $A_4 = 6, m = -2, \xi = 1, \xi_0 = 0, \kappa = 1, \tau = 1, \theta_0 = 0$.

Case 2

When $\Delta = 0$ and $m = 0$, Eq. (20) is $f(\omega) = \omega^3$, and the solution of Eq. (1) is

$$u_3 = \left(\pm\sqrt{\frac{2A_4}{3}}\right)^{-\frac{1}{3}} (\xi - \xi_0)^{\frac{1}{2}}\, \mathrm{e}^{i\left(\kappa\frac{x^\alpha}{\alpha} - \tau\frac{t^\alpha}{\alpha} - \theta_0\right)}. \tag{25}$$

Case 3

When $\Delta = 0$ and $m > 0$, Eq. (20) is $f(\omega) = \omega(\omega - \beta)^2$, and the solution of Eq. (1) is

$$u_4 = \left(\pm\sqrt{\frac{2A_4}{3}}\right)^{-\frac{1}{3}} \left[\frac{m}{2}\tan^2\left(\frac{1}{2}\sqrt{\frac{m}{2}}\left(\pm\sqrt{\frac{2A_4}{3}}\right)^{\frac{1}{3}}(\xi - \xi_0)\right)\right]^{\frac{1}{2}} \times \mathrm{e}^{i\left(\kappa\frac{x^\alpha}{\alpha} - \tau\frac{t^\alpha}{\alpha} - \theta_0\right)}. \tag{26}$$

Figure 8 illustrates the solution u_4 for different fractional orders $\alpha = 0.3$ and 0.8.

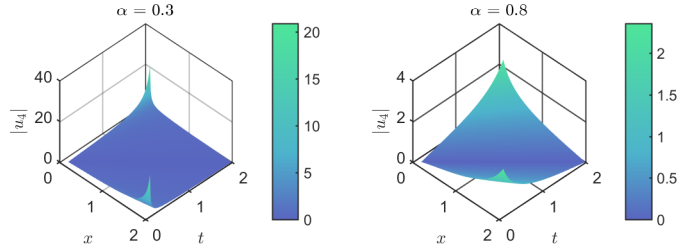


Fig. 8. Surface plots of the modulus $|u_4|$ under fixed parameters $A_4 = 6, m = 2, \xi = 1, \xi_0 = 0, \kappa = 1, \tau = 1, \theta_0 = 0$

Case 4

When $\Delta > 0$ and $n = 0$, Eq. (20) is $f(\omega) = \omega^2(\omega + \gamma)$. If $m > 0$, the solution of Eq. (1) is

$$u_5 = \left(\pm\sqrt{\frac{2A_4}{3}}\right)^{-\frac{1}{3}} \left[\frac{m}{2}\tanh^2\left(\frac{1}{2}\sqrt{\frac{m}{2}}\left(\pm\sqrt{\frac{2A_4}{3}}\right)^{\frac{1}{3}}(\xi-\xi_0)\right) - m\right]^{\frac{1}{2}} \times \mathrm{e}^{i\left(\kappa\frac{x^\alpha}{\alpha} - \tau\frac{t^\alpha}{\alpha} - \theta_0\right)}. \tag{27}$$

$$u_6 = \left(\pm\sqrt{\frac{2A_4}{3}}\right)^{-\frac{1}{3}} \left[\frac{m}{2}\coth^2\left(\frac{1}{2}\sqrt{\frac{m}{2}}\left(\pm\sqrt{\frac{2A_4}{3}}\right)^{\frac{1}{3}}(\xi-\xi_0)\right) - m\right]^{\frac{1}{2}} \times \mathrm{e}^{i\left(\kappa\frac{x^\alpha}{\alpha} - \tau\frac{t^\alpha}{\alpha} - \theta_0\right)}. \tag{28}$$

Figure 9 illustrates the solution u_5 for different fractional orders $\alpha = 0.3$ and 0.8, with $x = 1$ and $t = 3$.

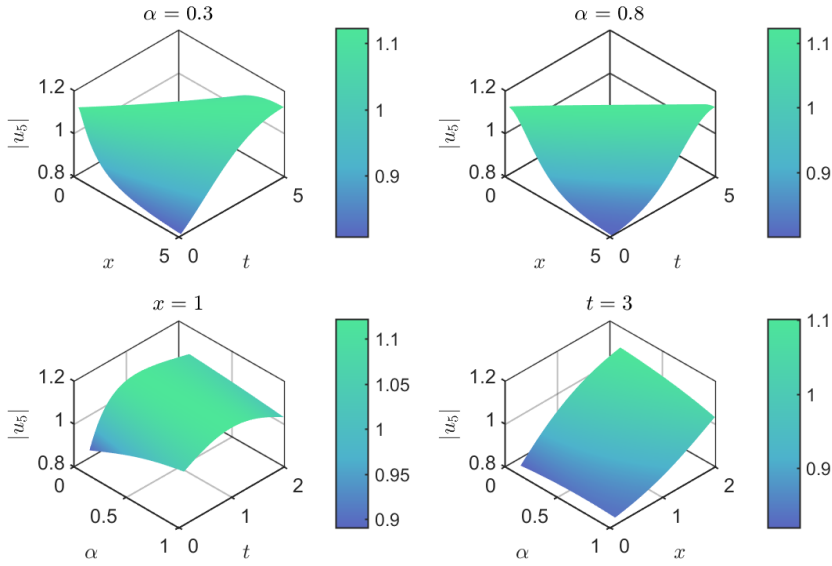


Fig. 9. Surface plots of the modulus $|u_5|$ under fixed parameters $A_4 = 6, m = 2, \xi = 1, \xi_0 = 0, \kappa = 1, \tau = 1, \theta_0 = 0$

Case 5

If $m<0$, the solution of Eq.(1) is

$$u_7 = \left(\pm\sqrt{\frac{2A_4}{3}}\right)^{-\frac{1}{3}}\left[-\frac{m}{2}\tan^2\left(\frac{1}{2}\sqrt{-\frac{m}{2}}\left(\pm\sqrt{\frac{2A_4}{3}}\right)^{\frac{1}{3}}(\xi-\xi_0)\right)-m\right]^{\frac{1}{2}} \times \mathrm{e}^{i\left(\kappa\frac{x^\alpha}{\alpha}-\tau\frac{t^\alpha}{\alpha}-\theta_0\right)}. \tag{29}$$

Case 6

When $\Delta>0$ and $n\neq 0$, Eq. (20) is $f(\omega)=\omega(\omega^2-m\omega-n)$, with γ_1, γ_2, γ_3 being its roots, one of which is 0, satisfying $\gamma_1<\gamma_2<\gamma_3$. If $\gamma_1<\omega<\gamma_2$, the solution of Eq. (1) is

$$u_8 = \left(\pm\sqrt{\frac{2A_4}{3}}\right)^{-\frac{1}{3}}\left[\gamma_1+(\gamma_2-\gamma_1)\,\mathrm{sn}^2\left(\frac{\sqrt{\gamma_3-\gamma_1}}{2}\right)\left(\pm\sqrt{\frac{2A_4}{3}}\right)^{\frac{1}{3}},r\right]^{\frac{1}{2}} \times \mathrm{e}^{i\left(\kappa\frac{x^\alpha}{\alpha}-\tau\frac{t^\alpha}{\alpha}-\theta_0\right)}, \tag{30}$$

if $\omega>\gamma_3$,

$$u_9 = \left(\pm\sqrt{\frac{2A_4}{3}}\right)^{-\frac{1}{3}}\left[\frac{\gamma_3-\gamma_2\,\mathrm{sn}^2\left(\frac{\sqrt{\gamma_3-\gamma_1}}{2}\left(\pm\sqrt{\frac{2A_4}{3}}\right)^{-\frac{1}{3}}(\xi-\xi_0),r\right)}{\mathrm{cn}^2\left(\frac{\sqrt{\gamma_3-\gamma_1}}{2}\left(\pm\sqrt{\frac{2A_4}{3}}\right)^{-\frac{1}{3}}(\xi-\xi_0),r\right)}\right]^{\frac{1}{2}} \times \mathrm{e}^{i\left(\kappa\frac{x^\alpha}{\alpha}-\tau\frac{t^\alpha}{\alpha}-\theta_0\right)}, \tag{31}$$

with $r^2=\frac{\gamma_2-\gamma_1}{\gamma_3-\gamma_1}$.

Figure 10 illustrates the solution u_8 for different fractional orders $\alpha=0.3$ and 0.8.

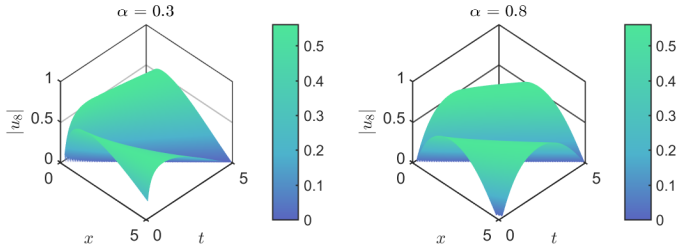


Fig. 10. Surface plots of the modulus $|u_8|$ under fixed parameters $A_4=6, \gamma_1=0, \gamma_2=0.5, \gamma_3=1, \xi=1, \xi_0=0, \kappa=1, \tau=1, \theta_0=0$.

Case 7

When $\Delta < 0$, Eq. (20) is $f(\omega) = \omega(\omega^2 - m\omega - n)$, and the solution of Eq. (1) is

$$u_{10} = \left(\pm\sqrt{\frac{2A_4}{3}}\right)^{-\frac{1}{3}} \left[-\sqrt{n} + \frac{2\sqrt{n}}{1 + \mathrm{cn}\left(n^{\frac{1}{4}}\left(\pm\sqrt{\frac{2A_4}{3}}\right)^{\frac{1}{3}}, r\right)}\right]^{\frac{1}{2}} \times \mathrm{e}^{i\left(\kappa\frac{x^\alpha}{\alpha} - \tau\frac{t^\alpha}{\alpha} - \theta_0\right)}, \tag{32}$$

with $r^2 = \frac{1}{2}(1 - \frac{m}{2\sqrt{n}})$.

Figure 11 illustrates the solution u_{10} for different fractional orders $\alpha = 0.3$ and 0.8, with $x = 1$ and $t = 3$.

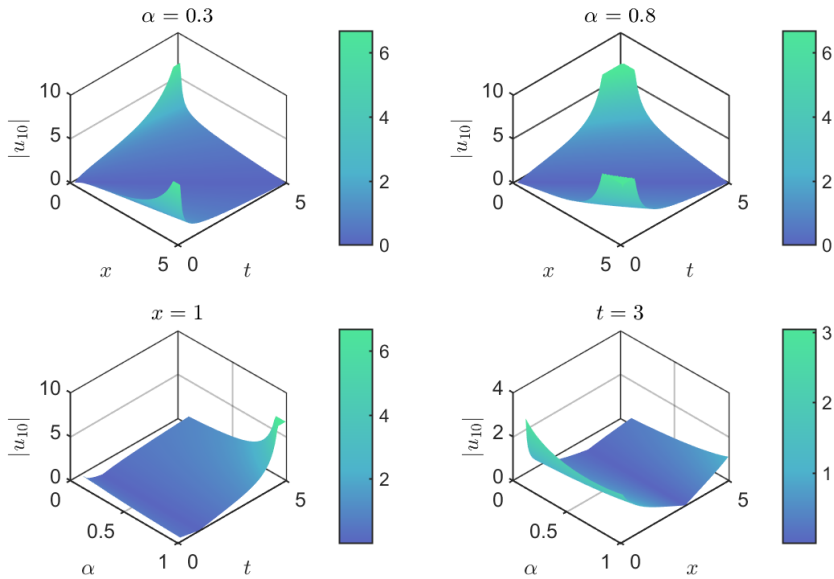


Fig. 11. Surface plots of the modulus $|u_{10}|$ under fixed parameters $A_4 = 6, m = 0, n = 1, \xi = 1, \xi_0 = 0, \kappa = 1, \tau = 1, \theta_0 = 0$.

We present three examples, focusing on the influence of α on the modulus of the solutions u_1, u_5, and u_{10} in Figs. 6, 9, and 11. There, we can clearly observe how variations in α affect $|u|$. In short, with different parameters, we have ten different solution families. We can obtain solutions that depend on appropriate physical parameters, thus improving the efficiency and accuracy of experiments. Furthermore, we can study the influence of different fractional-order parameters α on the solution.

5. Conclusion

This article analyzes solutions of the generalized nonlinear fractional SHE. Using the trial equation method, the equation is transformed into the ordinary differential equation. Then, the equation is changed into the planar dynamical system, and we analyze the existence of soliton solutions by utilizing bifurcation theory. Further, the system can exhibit chaotic behavior after introducing a perturbation term, which can be analyzed by calculating the LLE and observing chaos using three-dimensional phase portraits and time series plots. Liu's polynomial complete discriminant system yields ten families of solutions to the fourth-order equation. Meanwhile, the images of exact solutions can be observed under different fractional orders α. This research contributes to a deeper understanding of the propagation characteristics of ultrashort optical pulses in dispersion fibers and to the construction of the theory of fractional-order optical models. Compared with previous works, this paper has two advantages, which are the fractional-order generalization and the combination with solution-dynamics-chaos analysis. A limitation of the present study is that the chaotic analysis mainly relies on phase portraits, time series, and the LLE. Future work will study Poincaré sections, detailed sensitivity analysis, and stability analysis of solitons.

REFERENCES

[1] Y. Kai, Z. Yin, «Asymptotic analysis to domain walls between traveling waves modeled by real coupled Ginzburg–Landau equations», *Chaos Solit. Fractals* **152**, 111266 (2021).

[2] K.K. Ali *et al.*, «Optical soliton solutions, bifurcation analysis, chaotic behaviors of nonlinear Schrödinger equation and modulation instability in optical fiber», *Open Phys.* **23**, 20250164 (2025).

[3] F. Liu, Y. Feng, «The modified generalized Kudryashov method for nonlinear space-time fractional partial differential equations of Schrödinger type», *Results Phys.* **53**, 106914 (2023).

[4] Y. Yıldırım *et al.*, «Optical solitons in fibre Bragg gratings with third- and fourth-order dispersive reflectivities», *Ukr. J. Phys. Opt.* **22**, 239 (2021).

[5] S. Duran, D. Kaya, «Breaking analysis of solitary waves for the shallow water wave system in fluid dynamics», *Eur. Phys. J. Plus* **136**, 980 (2021).

[6] S. Duran, B. Karabulut, «Nematicons in liquid crystals with Kerr Law by sub-equation method», *Alex. Eng. J.* **61**, 1695 (2022).

[7] S. Duran, H. Durur, A. Yokuş, «Traveling wave and general form solutions for the coupled Higgs system», *Math. Methods Appl. Sci.* **46**, 8915 (2023).

[8] E.O. Adeyefa, E.O. Omole, A. Shokri, «Numerical solution of second-order nonlinear partial differential equations originating from physical phenomena using Hermite based block methods», *Results Phys.* **46**, 106270 (2023).

[9] H. Xin, «Optical envelope patterns in nonlinear media modeled by the Lakshmanan–Porsezian–Daniel equation», *Optik* **227**, 165839 (2021).

[10] N.A. Kudryashov, «Optical solitons of the Schrodinger–Hirota equation of the fourth order», *Optik* **274**, 170587 (2023).

[11] A.-M. Wazwaz, «The tanh method: Solitons and periodic solutions for the Dodd–Bullough–Mikhailov and the Tzitzeica–Dodd–Bullough equations», *Chaos Solit. Fractals* **25**, 55 (2005).

[12] A. Nazari-Golshan, «Investigation of Shock Waves in Nonextensive Electron–Positron–Ion Plasma with Relativistic Ions», *Plasma Phys. Rep.* **46**, 943 (2020).

[13] A. Bekir, A. Boz, «Exact solutions for nonlinear evolution equations using Exp-function method», *Phys. Lett. A* **372**, 1619 (2008).

[14] M. Mehdipoor, A. Neirameh, «New exact solutions for nonlinear solitary waves in Thomas–Fermi plasmas with (G'/G)-expansion method», *Astrophys. Space Sci.* **337**, 269 (2012).

[15] A. Nazari-Golshan, «Derivation and solution of space fractional modified Korteweg de Vries equation», *Commun. Nonlinear Sci. Numer. Simul.* **79**, 104904 (2019).

[16] P.M.A. Akbar, N. Ali, T. Islam, «Multiple closed form solutions to some fractional order nonlinear evolution equations in physics and plasma physics», *AIMS Math.* **4**, 397 (2019).

[17] A. Nazari-Golshan, «Fractional generalized Kuramoto–Sivashinsky equation: Formulation and solution», *Eur. Phys. J. Plus* **134**, 565 (2019).

[18] A. Nazari-Golshan, V. Fallahi, «Positron nonextensivity effect on the propagation of dust ion acoustic Gardner waves», *Z. Naturforsch. A* **76**, 965 (2021).

[19] H.M. Srivastava *et al.*, «Traveling wave solutions to nonlinear directional couplers by modified Kudryashov method», *Phys. Scr.* **95**, 075217 (2020).

[20] S.A. El-Wakil, E.M. Abulwafa, E.K. El-Shewy, A.A. Mahmoud, «Time-fractional Burgers equation for dust acoustic waves in a two different temperatures dusty plasma», *Astrophys. Space Sci.* **346**, 383 (2013).

[21] A. Nazari-Golshan, «Investigation of cylindrical shock waves in dusty plasma», *Indian J. Phys.* **92**, 1643 (2018).

[22] S.A. El-Wakil, E.M. Abulwafa, «Formulation and solution of space-time fractional Boussinesq equation», *Nonlinear Dyn.* **80**, 167 (2015).

[23] A. Nazari-Golshan, «Exploring new traveling wave solutions by solving the nonlinear space-time fractal Fornberg–Whitham equation», *Sci. Rep.* **14**, 18642 (2024).

[24] M. Iqbal, A.R. Seadawy, D. Lu, «Construction of solitary wave solutions to the nonlinear modified Kortewege–de Vries dynamical equation in unmagnetized plasma via mathematical methods», *Mod. Phys. Lett. A* **33**, 1850183 (2018).

[25] H. Rezazadeh, «New solitons solutions of the complex Ginzburg–Landau equation with Kerr law nonlinearity», *Optik* **167**, 218 (2018).

[26] N. Sene, «SIR epidemic model with Mittag–Leffler fractional derivative», *Chaos Solit. Fractals* **137**, 109833 (2020).

[27] H. Rezazadeh, M. Inc, D. Baleanu, «New Solitary Wave Solutions for Variants of (3+1)-Dimensional Wazwaz–Benjamin–Bona–Mahony Equations», *Front. Phys.* **8**, (2020).

[28] I. Onder *et al.*, «On solution of Schrodinger–Hirota equation with Kerr law via Lie symmetry reduction», *Nonlinear Dyn.* **111**, 19315 (2023).

[29] Z. Li, E. Zhu, «Optical soliton solutions of stochastic Schrodinger–Hirota equation in birefringent fibers with spatiotemporal dispersion and parabolic law nonlinearity», *J. Opt.* **53**, 1302 (2024).

[30] Y. Du, T. Yin, J. Pang, «The exact solutions of Schrodinger–Hirota equation based on the auxiliary equation method», *Opt. Quant. Electron.* **56**, 712 (2024).

[31] L. Tang, «Qualitative analysis, traveling wave solutions and chaotic behavior for the perturbed Schrödinger–Hirota equation with cubic-quintic-septic law of self-phase modulation», *Mod. Phys. Lett. B* **39**, 2550170 (2025).

[32] L. Tang, «Bifurcations and dispersive optical solitons for the nonlinear Schrödinger–Hirota equation in DWDM networks», *Optik* **262**, 169276 (2022).

[33] L. Tang, «Optical solitons perturbation and traveling wave solutions in magneto-optic waveguides with the generalized stochastic Schrödinger–Hirota equation», *Opti. Quant. Electron.* **56**, 773 (2024).

[34] L. Tang, Shanpeng Chen, «The classification of single traveling wave solutions for the fractional coupled nonlinear Schrödinger equation», *Opt. Quant. Electron.* **54**, 105 (2022).

[35] A. Sharif, «Jacobi elliptic function approach to a conformable fractional nonlinear Schrodinger–Hirota equation», *Partial Differ. Equ. Appl. Math.* **8**, 100541 (2023).

[36] M. ur Rahman, M. Sun, S. Boulaaras, D. Baleanu, «Bifurcations, chaotic behavior, sensitivity analysis, and various soliton solutions for the extended nonlinear Schrödinger equation», *Bound. Value Probl.* **2024**, 15 (2024).

[37] K. Hosseini, E. Hinçal, M. Ilie, «Bifurcation analysis, chaotic behaviors, sensitivity analysis, and soliton solutions of a generalized Schrödinger equation», *Nonlinear Dyn.* **111**, 17455 (2023).

[38] Z. Li, C. Huang, «Bifurcation, phase portrait, chaotic pattern and optical soliton solutions of the conformable Fokas–Lenells model in optical fibers», *Chaos Solit. Fractals* **169**, 113237 (2023).

[39] H. Zeng, L. Tang, «The Riemann–Hilbert approach and N-soliton solutions for the Schrödinger–Hirota equation in nonlinear optics», *Japan J. Ind. Appl. Math.* **43**, 32 (2026).

[40] L. Tang, «Qualitative Analysis: Chaotic Behavior and Optical Solitons Perturbation for the Coupled Foka–Lenells System in Birefringent Fibers», *Qual. Theory Dyn. Syst.* **24**, 59 (2025).

[41] L. Tang, «Bifurcation analysis, optical soliton solutions and chaotic pattern for the stochastic DWDM topology with spatio-temporal dispersion», *High Energy Density Phys.* **60**, 101292 (2026).

[42] L. Tang, «Bifurcation Analysis: Chaotic Behavior Cubic-Quartic Optical Solitons and Phase Portraits for the nonlinear Coupled Kaup–Newell Equation in Birefringent Fibers», *Math. Methods Appl. Sci.* **49**, 239 (2026).

[43] A.T. Ali, «New generalized Jacobi elliptic function rational expansion method», *J. Comput. Appl. Math.* **235**, 4117 (2011).

[44] C.-s. Liu, «Trial equation method and its applications to nonlinear evolution equations», *Acta Phys. Sin.* **54**, 2505 (2005).

[45] C.-s. Liu, «Using trial equation method to solve the exact solutions for two kinds of KdV equations with variable coefficients», *Acta Phys. Sin.* **54**, 4506 (2005).

[46] C.-s. Liu, «Trial Equation Method to Nonlinear Evolution Equations with Rank Inhomogeneous: Mathematical Discussions and Its Applications», *Commun. Theor. Phys.* **45**, 219 (2006).

[47] C.-s. Liu, «Applications of complete discrimination system for polynomial for classifications of traveling wave solutions to nonlinear differential equations», *Comput. Phys. Commun.* **181**, 317 (2010).

[48] A. Wolf, J.B. Swift, H.L. Swinney, J.A. Vastano, «Determining Lyapunov exponents from a time series», *Physica D* **16**, 285 (1985).

[49] Y. Kai, S. Chen, K. Zhang, Z. Yin, «A study of the shallow water waves with some Boussinesq-type equations», *Waves Random Complex Media* **34**, 1251 (2024).

[50] Y. Kai *et al.*, «Qualitative and quantitative analysis of nonlinear dynamics by the complete discrimination system for polynomial method», *Chaos Solit. Fractals* **141**, 110314 (2020).

[51] Y. Kai, J. Ji, Z. Yin, «Exact solutions and dynamic properties of Ito-Type coupled nonlinear wave equations», *Phys. Lett. A* **421**, 127780 (2022).

[52] Y. Li, Y. Kai, «Wave structures and the chaotic behaviors of the cubic-quartic nonlinear Schrödinger equation for parabolic law in birefringent fibers», *Nonlinear Dyn.* **111**, 8701 (2023).

[53] X. Wang, «Topological stability and patterns of traveling wave for a micro-polar non-Newtonian fluid model», *Mod. Phys. Lett. B* **35**, 2150237 (2021).

[54] X. Wang, «Stochastic exact solutions and averaging dynamical behaviors of the Hirota–Maccari system driven by multiplicative white noise», *Phys. Lett. A* **530**, 130078 (2025).

[55] X. Wang, H. Chen, D. Li, S. Fu, «Stochastic wave propagation dynamics and chaotic behavior under random perturbation for the fractional order Triki–Biswas model with white noise», *Chaos Solit. Fractals* **199**, 116612 (2025).

[56] X. Wang, «A comprehensive study on stochastic and chaotical dynamics for the random Radhakrishnan–Kundu–Lakshmanan optical model», *Phys. Lett. A* **567**, 131209 (2026).